J Cancer Res Clin Oncol (2016) 142:619–632
DOI 10.1007/s00432-015-2067-2

ORIGINAL ARTICLE – CANCER RESEARCH

Radionuclide therapy using ^{131}I-labeled anti-epidermal growth factor receptor-targeted nanoparticles suppresses cancer cell growth caused by EGFR overexpression

Wei Li[1] · Zhongyun Liu[2] · Chengxia Li[1] · Ning Li[1] · Lei Fang[3] · Jin Chang[3] · Jian Tan[1]

Received: 7 July 2015 / Accepted: 23 October 2015 / Published online: 16 November 2015

Abstract

Introduction Anti-epidermal growth factor receptor (EGFR)-targeted nanoparticles can be used to deliver a therapeutic and imaging agent to EGFR-overexpressing tumor cells. ^{131}I-labeled anti-EGFR nanoparticles derived from cetuximab were used as a tumor-targeting vehicle in radionuclide therapy.

Methods This paper describes the construction of the anti-EGFR nanoparticle EGFR–BSA–PCL. This nanoparticle was characterized for EGFR-targeted binding and cellular uptake in EGFR-overexpressing cancer cells by using flow cytometry and confocal microscopy. Anti-EGFR and non-targeted nanoparticles were labeled with ^{131}I using the chloramine-T method. Analyses of cytotoxicity and targeted cell killing with ^{131}I were performed using the MTT assay. The time-dependent cellular uptake of ^{131}I-labeled anti-EGFR nanoparticles proved the slow-release effects of nanoparticles. A radioiodine therapy study was also performed in mice.

Results The EGFR-targeted nanoparticle EGFR–BSA–PCL and the non-targeted nanoparticle BSA–PCL were constructed; the effective diameters were approximately 100 nm. The results from flow cytometry and confocal microscopy revealed significant uptake of EGFR–BSA–PCL in EGFR-overexpressing tumor cells. Compared with EGFR–BSA–PCL, BSA–PCL could also bind to cells, but tumor cell retention was minimal and weak. In MTT assays, the EGFR-targeted radioactive nanoparticle ^{131}I–EGFR–BSA–PCL showed greater cytotoxicity and targeted cell killing than the non-targeted nanoparticle ^{131}I–BSA–PCL. The radioiodine uptake of both ^{131}I-labeled nanoparticles, ^{131}I–EGFR–BSA–PCL and ^{131}I–BSA–PCL, was rapid and reached maximal levels 4 h after incubation, but the ^{131}I uptake of ^{131}I–EGFR–BSA–PCL was higher than that of ^{131}I–BSA–PCL. On day 15, the average tumor volumes of the ^{131}I–EGFR–BSA–PCL and ^{131}I–BSA–PCL groups showed a slow growth relationship compared with that of the control group.

Conclusion The EGFR-targeted nanoparticle EGFR–BSA–PCL demonstrated superior cellular binding and uptake compared with those of the control BSA–PCL. The EGFR-targeted radioactive nanoparticle ^{131}I–EGFR–BSA–PCL exhibited favorable intracellular retention of ^{131}I. Radionuclide therapy using ^{131}I–EGFR–BSA–PCL, which showed excellent targeted cell killing, suppressed cancer cell growth caused by EGFR overexpression.

Keywords Epidermal growth factor receptor · Nanoparticles · ^{131}I · Radioiodine therapy · Tumor-targeting

Wei Li and Zhongyun Liu have contributed equally to this work.

✉ Jian Tan
tanpost@163.com

[1] Department of Nuclear Medicine, Tianjin Medical University General Hospital, Anshan Road 154, Heping District, Tianjin 300052, People's Republic of China

[2] Yantai Institute of Coastal Zone Research, Chinese Academy of Sciences, Yantai 264003, Shandong, People's Republic of China

[3] Institute of Nanobiotechnology, School of Materials Science and Engineering, Tianjin Key Laboratory of Composites and Functional Materials, Tianjin University, Tianjin 300072, People's Republic of China

Introduction

Nanoparticles, including liposomes and other nanoscale constructs, can be used to combine a therapeutic agent

with an imaging agent, thereby allowing direct monitoring of drug delivery to tumors. The size of fenestrations in the tumor endothelium allows nanoparticles to pass from the circulation into the tumor interstitium where they can access cancer cells. Furthermore, molecules may also become trapped in this interstitium, which is a phenomenon generally referred to as the enhanced permeability and retention effect (Saha et al. 2010). Several types of nanoparticles, such as metal-, polymer-, and lipid-based nanoparticles, have been developed to deliver therapeutic agents, including chemotherapeutic agents, radionuclides, photosensitizers, and siRNA. Targeting ligands/moieties, such as peptides, antibodies, or antibody fragments, can be attached to nanoparticles to improve therapeutic efficacy (Hussain et al. 2013). In an attempt to increase specificity, liposomes, which are spherical vesicles formed by lipid bilayers, have been conjugated to monoclonal antibodies or antibody fragments for specific delivery to target cells. Studies have shown that antibody-conjugated liposomes caused significant tumor cytotoxicity and growth inhibition compared with non-targeted liposomes, making them a promising tool for future treatment in oncology (Pastorino et al. 2003).

Epidermal growth factor receptor (EGFR) is one of the four members of the epidermal growth factor receptor family. It plays an important role in the proliferation, apoptosis, dedifferentiation, angiogenesis, invasion, and metastasis of tumor cells. As reported by some studies, 40–80 % of non-small cell lung cancers (NSCLC) (Chen et al. 2012), 20–25 % of breast cancers (Capelan et al. 2013), 35–40 % of colorectal cancers (Normanno et al. 2009), and 80–90 % of head and neck squamous cell carcinomas (HNSCC) (Ang et al. 2002) showed EGFR overexpression. Molecular imaging and targeted therapy against EGFR are significant areas in cancer research, and several monoclonal antibodies against EGFR are available. The most advanced clinical member of this drug class is cetuximab (IMC-C225 or Erbitux; ImClone Systems Inc., NY, USA/Merck KGaA, Darmstadt, Germany), which competitively inhibits binding to both EGFR and EGFRvIII; cetuximab is the first FDA-approved EGFR-specific mAb for the treatment of patients with EGFR-expressing metastatic colorectal and head/neck cancers (Giaccone 2005). Anti-EGFR immunoliposomes have already been produced (Mamot et al. 2003).

Radioiodine therapy for differentiated thyroid carcinoma has been used for numerous years. Radioiodine kills not only sodium iodide symporter-expressing cells but also adjacent tumor cells because of the cross-fire effect of radiation therapy. In this paper, we describe the construction of ^{131}I-labeled anti-EGFR nanoparticles derived from cetuximab as a tumor-targeting vehicle for radionuclide therapy. These nanoparticles were characterized for cellular uptake, cytotoxicity, targeted cell killing with ^{131}I, and time-dependent cellular uptake of ^{131}I in breast cancer, colorectal cancer, NSCLC, and HNSCC cells in vitro; we also performed a radioiodine therapy study in NCI-H1972 NSCLC xenograft nude mice by intratumoral injection of nanoparticles in vivo.

Materials and methods

Materials

Reagents were obtained from the following sources: Dulbecco's modified Eagle's medium (DMEM) (Gibco), Roswell Park Memorial Institute (RPMI) 1640 medium (Gibco), Minimum Essential Medium Eagles with Earle's Balanced Salts (MEM-EBSS) (Gibco), fetal bovine serum (FBS) (Gibco), rabbit polyclonal antihuman epidermal growth factor receptor antibody (Abcam, ab2430), and 5 mg/mL monoclonal antibody (MERCK Inc., C225, cetuximab).

Cell lines

The NSCLC cell lines NCI-H292 and NCI-H1975; breast cancer cell lines MDA-MB-231, MDA-MB-453, and MDA-MB-468; colorectal cancer cell line LS180; and squamous cell carcinoma cell line A431 were purchased from Cell Resource Center, Institute of Basic Medical Sciences, Chinese Academy of Medical Sciences/Peking Union Medical College (Beijing, China); EGFR was overexpressed in all of these cell lines (Mamot et al. 2003, 2006; Nagaria et al. 2013; Zhou et al. 2012). The cell lines MDA-MB-231, MDA-MB-453, MDA-MB-468, and A431 were cultured in DMEM supplemented with 10 % FBS and 1 % penicillin/streptomycin. The cell lines NCI-H292 and NCI-H1975 were cultured in RPMI 1640 medium supplemented with 10 % FBS and 1 % penicillin/streptomycin. The cell line LS180 was cultured in MEM-EBSS medium supplemented with 10 % FBS and 1 % penicillin/streptomycin. The cell cultures were stored in a humidified atmosphere containing 5 % CO_2 buffered with ambient air at 37 °C.

Preparation, conjugation, and characterization of nanoparticles (Liu et al. 2014)

The amphiphilic BSA–PCL conjugate was synthesized as previously described (Liu et al. 2014), and the nanosized self-assembled amphiphilic BSA–PCL conjugate was obtained via the emulsion–solvent evaporation method (Du et al. 2013). Briefly, 4 mg of BSA–PCL conjugate was dissolved in 4 mL of phosphate buffer (PB, 0.1 M, pH 7.4) at room temperature and activated with *N*-(3-dimethyl amino

propyl)-3-2 ethyl carbon imine hydrochloride (EDC) and *N*-hydroxy succinimide (NHS) for 15 min, to which 5 mg/mL cetuximab antibodies were added (100 μg cetuximab antibodies per 1 mg BSA–PCL) at 4 °C overnight. The obtained PB solutions of the self-assemblies of the BSA–PCL conjugate and the cetuximab-decorated BSA–PCL conjugate EGFR–BSA–PCL were stored at 4 °C. The EGFR–BSA–PCL and BSA–PCL conjugates were synthesized by Liu Zhongyun, Ph.D., and Professor Chang Jin from TianJin University, Department of Polymer Materials Science and Engineering (Liu et al. 2014). Nanoparticles were dissolved in 10 % Triton X-100 for measurement of BSA and cetuximab antibody content by high-performance liquid chromatography (HPLC) (Chen et al. 2015). Measurement of the amount of antibody per nanoparticle was performed by the ratio of their surface areas; the BSA and EGFR protein qualification were performed by high-performance liquid chromatography (HPLC), and the detailed description is provided by in Kao et al. (2013) and Cho et al. (2010).

Nanoparticle targeting in EGFR overexpression cell lines (Cho et al. 2010; Du et al. 2013; Kao et al. 2013)

The cellular binding and uptake of two different nanoparticles, EGFR–BSA–PCL and BSA–PCL, were evaluated by confocal microscopy and flow cytometry in seven EGFR-overexpressing cell lines (MDA-MB-231, MDA-MB-453, MDA-MB-468, NCI-H292, NCI-H1975, LS180, and A431). The nanoparticles were added at a concentration of 1 mg/10^6 cells and incubated for 4 h at 37 °C. After incubation, the cells were washed three times with PBS, fixed with 4 % paraformaldehyde, and analyzed by confocal microscopy (laser scanning confocal microscope; Olympus FV1000, Japan).

Flow cytometry was used to quantify the targeting potential of the nanoparticles. Flow cytometry was performed using a FACScan Cytometer (BD FACSCalibur; BD Biosciences, USA) by counting 30,000 events, and the data were analyzed using FlowJo software. The experiments were performed as follows: nanoparticles were added at a concentration of 1 mg/10^6 cells and incubated for 4 h at 37 °C. After incubation, 5 × 10^6 cells were washed twice with 500 μL of PBS buffer by centrifugation (2000 rpm for 10 min), and a 250-μL cell suspension was obtained. Another 250 μL of 4 % paraformaldehyde was then added and analyzed by flow cytometry.

Direct labeling (Nordberg et al. 2007)

EGFR–BSA–PCL and BSA–PCL were labeled with ^{131}I (Beijing atomic Hi-tech Co., Ltd.) using the chloramine-T method. Approximately 100 μg of EGFR–BSA–PCL or BSA–PCL was diluted in PB to a total volume of 100 μL, and ~74 MBq ^{131}I was added. Chloramine-T (100 μL; 5 mg/mL in PB) was added. After 60 s of shaking and incubation, the reaction was stopped by adding 100 μL of sodium metabisulfite (5 mg/mL in PB). To separate labeled EGFR–BSA–PCL and BSA–PCL from low molecular weight compounds, a centrifuge tube (Amicon® Pro Purification System, Merck Millipore) was used. The specific radioactivity was approximately 370–690 MBq/mg for ^{131}I–EGFR–BSA–PCL and ^{131}I–BSA–PCL. The labeling rate of ^{131}I was approximately 50–85 %.

Competitive effect study in vitro (Du et al. 2013)

To further investigate the competitive effect of EGFR on the uptake of the nanoparticles, tumor cells were seeded in 24-well plates overnight and were incubated with ^{131}I–EGFR–BSA–PCL and ^{131}I–BSA–PCL for 1 h; radioactivity was measured using a γ counter (LKB gamma 1261; LKB Instruments). Next, 500 μL rhEGF (0.2 ng/mL, Promega, USA) was added to these cells for 1 h, and then tumor cells were incubated with ^{131}I–EGFR–BSA–PCL for another 1 h. After incubation, cells were washed three times with PBS before radioactivity was measured.

Western blot analysis

For Western blot analysis, the PS 2A200 electrophoresis system (Amersham Biosciences, USA) was used. Membranes were incubated with EGFR (dilution 1:1000, sc-120, Abcam, USA) or β-actin (dilution 1:1000, TA-09, Novus Biologicals, USA) antibodies for 2 h at room temperature. The membranes were then incubated with secondary antibodies at room temperature for another 1 h and covered with Pierce ECL Western Blotting Substrate (Thermo Fisher Scientific, USA) at room temperature for 1 min and exposed to Fuji X-ray film in the darkroom. Prestained protein molecular weight standards (Spectra Multicolor Broad Range Protein Ladder, SM1841, Fermentas, Germany) were run in the same gels for molecular weight comparison and estimation of transfer efficiency.

Cell killing with ^{131}I and MTT assay (Chung et al. 2011)

To examine the effects of ^{131}I–EGFR–BSA–PCL and ^{131}I–BSA–PCL on cell growth, tumor cells were seeded in 96-well plates at 1 × 10^4 cells per well overnight and were incubated with ^{131}I–EGFR–BSA–PCL or ^{131}I–BSA–PCL under different concentration doses for 4 h. All of the nanoparticles were then wiped off, and the cells were incubated for another 24 h. To examine whether radionuclide nanoparticles can kill tumor cells, the cells were extensively washed twice with PBS, and 20 μL of MTT reagent

(5.0 mg/mL) [3-(4, 5 dimethylthiazol-2-yl)-2, 5-diphenyl tetrazolium bromide; Sigma] was added to each well for 4 h. The amount of formazan blue compound indicates the number of living cells and was determined using a spectrophotometer (BioTek, ELX800, USA) at $\lambda = 492$ nm.

Time-dependent cellular uptake of ^{131}I–EGFR–BSA–PCL and ^{131}I–BSA–PCL (Nordberg et al. 2007)

To measure the time-dependent cellular uptake of ^{131}I-labeled nanoparticles, 1×10^5 cells per well were seeded in 96-well plates and cultured with 3.7 MBq/mL ^{131}I–EGFR–BSA–PCL, ^{131}I–BSA–PCL, or ^{131}I. The cells were washed, lysed with 0.3 M sodium hydroxide, and counted every 2 h for 4 h, every 4 h until 12 h, and then every 6 h until 24 h. Radioactivity was measured using a γ counter (LKB gamma 1261; LKB Instruments). All of the experiments were performed in triplicate. ^{131}I could not be retained in non-thyroid cells, so these cells comprised the control group.

Animal model

Experimental animals were purchased from the Beijing Experimental Animal Center of Peking Union Medical, China. The generation of subcutaneous tumors was performed as follows: a 5×10^6 NCI-H1972 tumor cell suspension in 50 μL of DMEM was subcutaneously injected into the right shoulder of 4-week-old BALB/c female nude mice weighing 19–21 g. Mice were kept under specific pathogen-free conditions at the Laboratory Animal Center, Tianjin Medical University, China. The animal experiment guidelines were followed according to the regulations of Swiss veterinary law. The results were similar to those of the in vitro clonogenic assay in MDA-MB-231, MDA-MB-453, MDA-MB-468, NCI-H292, NCI-H1975, LS180, and A431 EGFR-overexpressing tumor cells. Therefore, NCI-H1972 cells were selected for animal testing. For the therapeutic experiments, all 20 mice were divided into four groups in terms of the ^{131}I-labeled EGFR-targeted nanoparticle ^{131}I–EGFR–BSA–PCL, the ^{131}I-labeled non-targeted nanoparticle ^{131}I–BSA–PCL, the EGFR-targeted nanoparticle EGFR–BSA–PCL, and the non-targeted nanoparticle BSA–PCL.

Tissue distribution of ^{131}I, ^{131}I–EGFR–BSA–PCL, and ^{131}I–BSA–PCL

The mice bearing human cancer were used for the biodistribution study at day 21 after tumor inoculation. The mice in each group were killed at 24 and 72 h post-injection with the respective drugs. The heart, spleen, liver, colon, and tumor samples were collected for weighing and for radioactivity measurements with a γ counter (LKB gamma 1261; LKB Instruments). Meanwhile, the remaining spleen, liver, and tumor tissues were collected to study the histopathology of each group. Data were expressed as each gram of tissue (% ID/g) (Li et al. 2004).

Radioiodine therapy study in mice

When the tumors reached a minimum size of 10 mm in diameter, 74 MBq (370 MBq/mL) ^{131}I–EGFR–BSA–PCL, 74 MBq (370 MBq/mL) ^{131}I–BSA–PCL, 1 mg (20 mg/mL) EGFR–BSA–PCL, or 1 mg (20 mg/mL) BSA–PCL was injected into the tumor. The tumor size was monitored prior to the administration of radioiodine and every 3 days thereafter by measuring three diameters with a sliding caliper and converting the diameter to the volume using the formula $V = 4\pi abc/3$. Control groups were followed to day 15 after injection and then killed due to excessive tumor burden by cervical dislocation under deep isoflurane sedation. The therapy groups were followed to day 35 after injection and were then killed.

Statistical analysis

All of the experiments were performed in triplicate unless otherwise indicated in vitro. Statistical analysis was conducted using SPSS software version 13.0. The results are presented as the mean ± SD. Statistical significance was tested using Student's *t* test or ANOVA.

Results

Size and morphology of BSA–PCL and EGFR–BSA–PCL

The size and morphology of the resulting BSA–PCL and EGFR–BSA–PCL were measured by a laser particle size analyzer and transmission electron microscopy (TEM). TEM analyses (insets of Fig. 1) of BSA–PCL and EGFR–BSA–PCL showed that the shape of the BSA carrier was retained after modification. They were both well-dispersed nanoparticles with a spherical shape. The DLS measurement showed the average diameter was approximately 130–180 nm and the polydispersity index (PDI) was 0.164, in agreement with the TEM result. The mean ζ potential of the obtained protein-based vesicle was also measured, with a value of −38.70 mV. The negative surface charge that resulted from the BSA shell could reduce undesired protein adsorption and provide good protection for the vesicle during circulation in the body. The diameter of nanoparticle EGFR–BSA–PCL was approximately 180 nm, the radius of BSA was 3.5 nm, the hydronamic radius of antibody

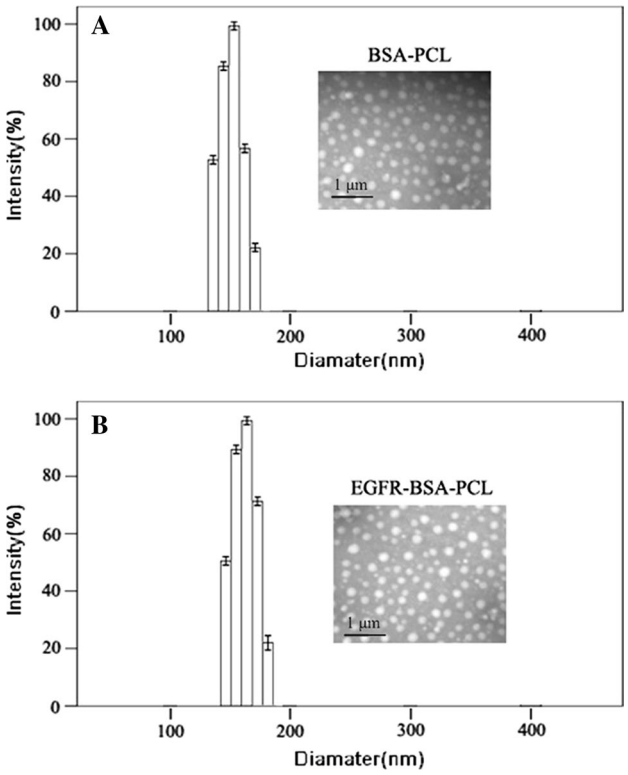

Fig. 1 Diameter and TEM imaging of the self-assembly of the BSA–PCL (**a**) and EGFR–BSA–PCL (**b**) conjugates. The effective diameters of BSA–PCL (**a**) and EGFR–BSA–PCL (**b**) were approximately 100 nm, as shown. TEM analyses of BSA–PCL and EGFR–BSA–PCL showed that the shape of the BSA carrier was retained after modification

C225 was 1.5 nm; so, the surface area of the nanoparticle was 101,736 nm^2, and the cross-sectional area of C225 and BSA were 7.1 and 38.5 nm^2, respectively. According to the ratio of BSA and C225 measured by HPLC, the amount of antibody per nanoparticle was estimated to be approximately 3800 antibody molecules per nanoparticle.

Internalization of EGFR–BSA–PCL and BSA–PCL

Confocal microscopy was used to evaluate the binding of EGFR–BSA–PCL and BSA–PCL to target tumor cells with high EGFR expression. We investigated their targeting abilities against different cancer cells. Figure 2 shows the confocal images of MDA-MB-231, MDA-MB-453, MDA-MB-468, NCI-H292, NCI-H1975, LS180, and A431 cancer cells incubated with EGFR–BSA–PCL and BSA–PCL. Immunofluorescence (Fig. 2) showed that EGFR–BSA–PCL was significantly internalized in EGFR-overexpressed tumor cells and exhibited strong green fluorescence. Compared with EGFR–BSA–PCL, BSA–PCL could also bind to cells, but tumor cell retention was minimal and the binding green fluorescence was weak. This result suggests that the targeting ability of nanoparticles was enhanced via modification with anti-EGFR antibody.

Flow cytometry of nanoparticle binding and cellular uptake

Fluorescence-activated cell-sorting analyses revealed results consistent with those observed in confocal microscopy analyses, showing a significant uptake of EGFR–BSA–PCL. As shown in Fig. 3, rapid and efficient binding of EGFR–BSA–PCL to EGFR-overexpressing target cell lines was demonstrated. The binding and uptake of EGFR–BSA–PCL were higher than those of non-targeted nanoparticles in MDA-MB-231, MDA-MB-453, MDA-MB-468, NCI-H292, NCI-H1975, LS180, and A431 cell lines ($p < 0.05$). This finding implies that EGFR–BSA–PCL had a special binding efficiency with tumor cells expressing EGFR.

Competitive effect study in vitro

After rhEGF was added to these cells for 1 h, radioiodide uptake in the rhEGF + ^{131}I–EGFR–BSA–PCL group was lower than the ^{131}I–EGFR–BSA–PCL group. The results showed that rhEGF bound to EGFR receptors on the surfaces of tumor cells, C225-mediated endocytosis of nanoparticles was restrained, the endocytosis of ^{131}I–EGFR–BSA–PCL was also restrained, and radioiodide uptake was depressed in EGFR-overexpressing tumor cells (Fig. 4).

Targeted cell killing with ^{131}I

The EGFR expression was assayed by Western blot in Fig. 5. The EGFR proteins in MDA-MB-231, MDA-MB-453, MDA-MB-468, NCI-H292, NCI-H1975, LS180, and A431 cancer cells were detected as major bands corresponding to a molecular weight at 170 kDa. The β-actin protein was used as a positive control and expressed in all cells as a major band with a molecular weight at 43 kDa.

For studies on cell killing with ^{131}I, EGFR–BSA–PCL and BSA–PCL were labeled with ^{131}I for targeted delivery to EGFR- or EGFRvIII-overexpressing cells. ^{131}I–EGFR–BSA–PCL and ^{131}I–BSA–PCL were incubated with various cell lines and compared with ^{131}I to evaluate the efficiency and specificity of targeted cell killing. In recent studies, a similar treatment with the antihuman EGFR antibody C225 showed no cytotoxicity using the MTT assay (Mamot et al. 2003). EGFR–BSA–PCL and BSA–PCL also showed no cytotoxicity using the MTT assay (Liu et al. 2014). Furthermore, nanoparticles containing C225-Fab, but lacking an encapsulated drug, similarly showed no cytotoxicity under these MTT assay conditions (Mamot et al. 2003). Thus, ^{131}I–EGFR–BSA–PCL and ^{131}I–BSA–PCL were compared with ^{131}I to confirm EGFR-targeted cell killing using MTT assays.

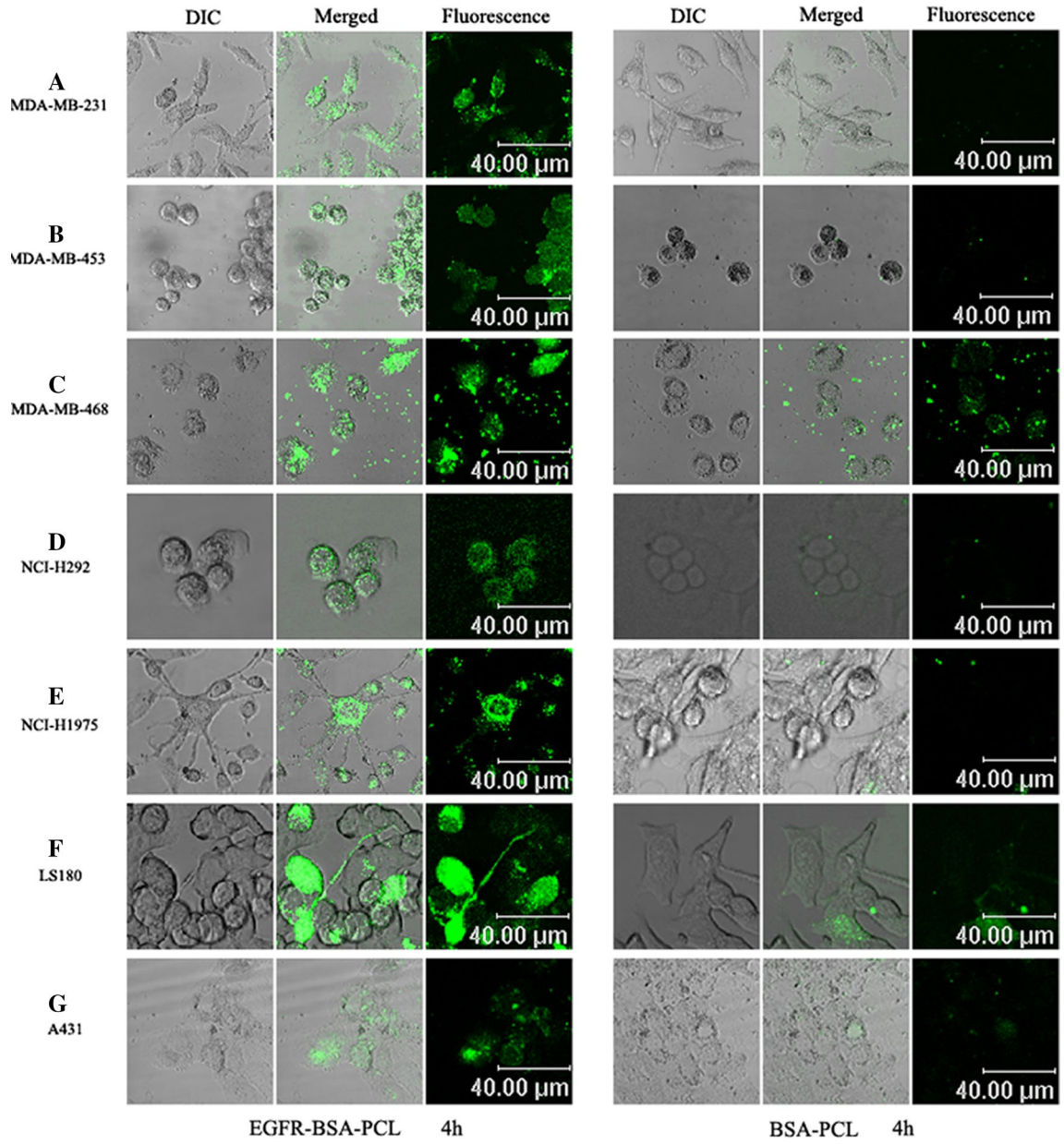

Fig. 2 Confocal microscopy images of cancer cells incubated with BSA–PCL or EGFR–BSA–PCL for 4 h. Immunofluorescence showed that EGFR–BSA–PCL was significantly internalized in EGFR-overexpressed MDA-MB-231 (**a**), MDA-MB-453 (**b**), MDA-MB-468 (**c**), NCI-H292 (**d**), NCI-H1975 (**e**), LS180 (**f**), and A431 (**g**) tumor cells and exhibited strong green fluorescence. Compared with EGFR–BSA–PCL, BSA–PCL could also bind to cells, but tumor cell retention was minimal and the green fluorescence binding was weak

Compared with the non-targeted nanoparticle ^{131}I–BSA–PCL, the EGFR-targeted radionuclide nanoparticle ^{131}I–EGFR–BSA–PCL showed greater cytotoxicity in vitro, indicating that the delivery was antibody dependent. In MDA-MB-231, MDA-MB-453, and MDA-MB-468 breast cancer cells, ^{131}I–EGFR–BSA–PCL showed substantial in vitro cytotoxicity after treatment for 4 h. The IC50 values of ^{131}I–EGFR–BSA–PCL in MDA-MB-231, MDA-MB-453, and MDA-MB-468 breast cancer cells were 0.31 (Fig. 6a), 0.34 (Fig. 6b), and 0.04 MBq/mL (Fig. 6c), respectively, whereas those of ^{131}I–BSA–PCL were 0.71 (Fig. 6a), 0.39 (Fig. 4b), and 0.25 MBq/mL (Fig. 6c), respectively. Meanwhile, the IC50 values of ^{131}I–EGFR–BSA–PCL in NSCLC cell lines NCI-H292 and NCI-H1972 were 0.70 (Fig. 6e) and 0.70 MBq/mL (Fig. 6f), respectively, whereas those of ^{131}I–BSA–PCL were 1.8 (Fig. 6e) and 3.26 MBq/mL (Fig. 6f), respectively. The IC50 values of ^{131}I–EGFR–BSA–PCL in the colorectal cancer cell line LS180 and squamous cell carcinoma cell line A431 were 1.32 (Fig. 6d) and 0.03 MBq/mL (Fig. 6g), respectively,

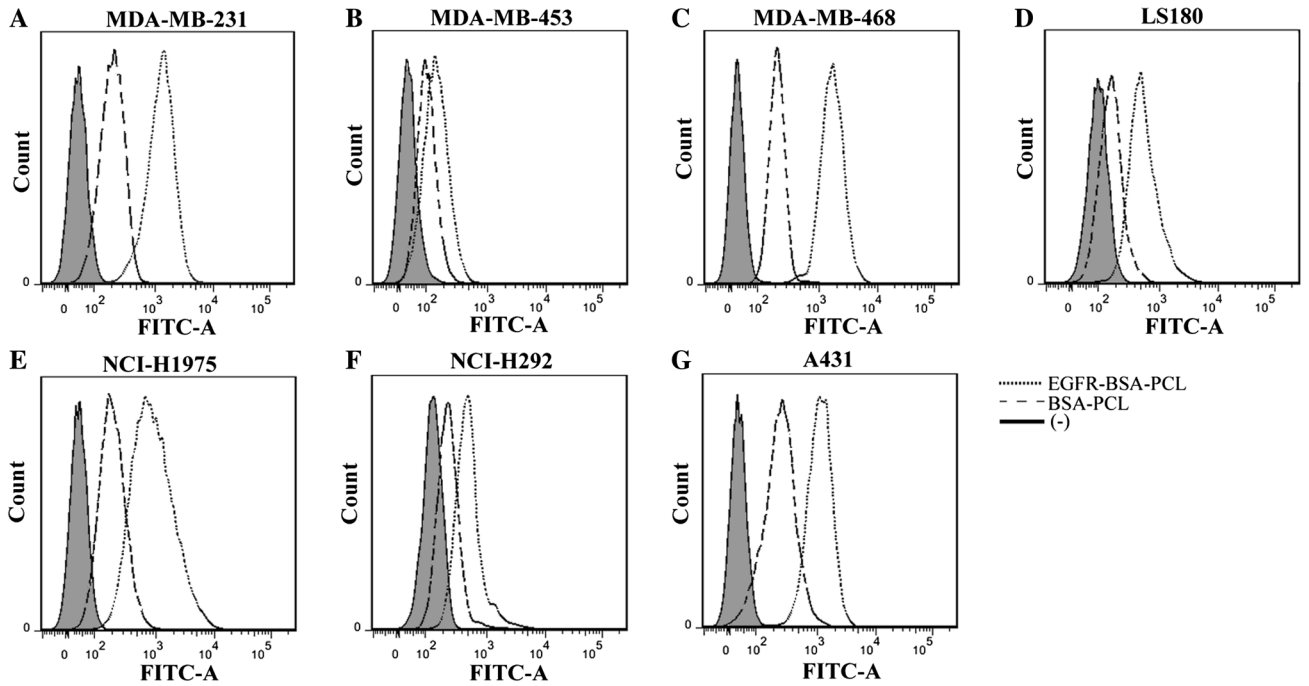

Fig. 3 Binding activity of EGFR–BSA–PCL and BSA–PCL to target cell lines. In MDA-MB-231 (**a**), MDA-MB-453 (**b**), MDA-MB-468 (**c**), LS180 (**d**), NCI-H1975 (**e**), NCI-H292 (**f**), and A431 (**g**) tumor cells, rapid and efficient binding of EGFR–BSA–PCL to EGFR-over-expressing target cell lines was demonstrated (*$p < 0.05$, compared with BSA–PCL)

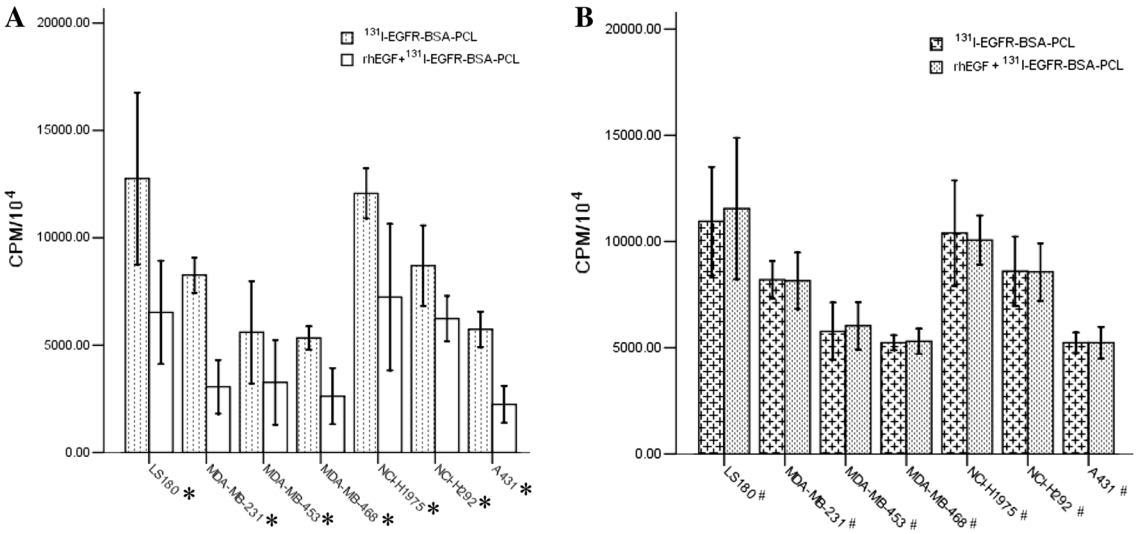

Fig. 4 Competitive effect study in vitro. After incubation, ^{131}I–EGFR–BSA–PCL (**a**) and ^{131}I–BSA–PCL (**b**) were measured using a γ counter (*$p < 0.01$, compared with rhEGF + ^{131}I–EGFR–BSA–PCL, $^{\#}p > 0.5$, compared with rhEGF + ^{131}I–BSA–PCL)

whereas those of ^{131}I–BSA–PCL were 12.19 (Fig. 6d) and 0.32 MBq/mL (Fig. 6g), respectively. The survival rates of tumor cells not incubated with ^{131}I that were only incubated with ^{131}I were similar because non-thyroid tumor cells could not uptake ^{131}I; thus, ^{131}I retention was too short to kill the cells, as shown in Fig. 6.

Time-dependent cellular uptake

To determine the iodide uptake of ^{131}I–EGFR–BSA–PCL and ^{131}I–BSA–PCL, ^{131}I-timed activity measurements were obtained in MDA-MB-231, MDA-MB-453, MDA-MB-468, LS180, NCI-H1975, NCI-H292, and A431 tumor

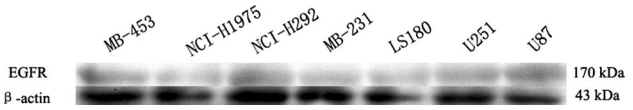

Fig. 5 Western blot analysis. The EGFR proteins in MDA-MB-231, MDA-MB-453, MDA-MB-468, NCI-H292, NCI-H1975, LS180, and A431 cancer cells were 170 kDa. The β-actin protein was used as positive control and expressed in all cells at 43 kDa

cells in Fig. 7a–g. Radioiodide uptake in those cells was rapid, reaching maximal levels 4 h after incubation with ^{131}I–EGFR–BSA–PCL and ^{131}I–BSA–PCL; ^{131}I uptake of ^{131}I–EGFR–BSA–PCL was higher than that of ^{131}I–BSA–PCL as shown in Fig. 7h. Cell-associated ^{131}I activity after 24 h was still very high and almost 79–84 % in all seven cell lines because of the slow-release effect of internalized nanoparticles from cells.

Radioiodine therapy study in mice

Figure 8a shows the average tumor volume progression for the two ^{131}I-nanoparticle therapy groups and the two corresponding unlabeled nanoparticle control groups. Injection on day 3 was used as the initial reference due to the significant tumor swelling on day 1 and day 2. On day 35, the average tumor volumes of the ^{131}I–EGFR–BSA–PCL and ^{131}I–BSA–PCL groups were 329.7 ± 135.2 and 365.6 ± 113.8 %, respectively. On day 15, the average tumor volumes of the ^{131}I–EGFR–BSA–PCL and ^{131}I–BSA–PCL groups were 180.9 ± 107.5 and 205.7 ± 25.2 %, respectively, indicating slow growth. In comparison, tumors in the EGFR–BSA–PCL and BSA–PCL nanoparticle control groups showed rapid growth, with tumor volumes of 272.7 ± 138.1 and 312.2 ± 182.8 %, respectively, at day 15.

The tissue distribution of ^{131}I–EGFR–BSA–PCL in nude mice was measured by γ counts in Fig. 8b. ^{131}I–EGFR–BSA–PCL was markedly absorbed by tumor tissues. Among the non-tumor tissues, ^{131}I–EGFR–BSA–PCL was mostly accumulated in the liver and spleen. The levels of ^{131}I–EGFR–BSA–PCL and ^{131}I–BSA–PCL in tumor tissues were significantly higher than in the other two groups at 24 and 72 h after treatment.

Discussion

Tumor-targeting therapy has overcome the lack of specificity of traditional therapeutic agents. Liposomes, which are spherical vesicles formed by lipid bilayers, have been widely investigated as carriers of tumor-targeting therapeutic agents. Some specific ligands have been conjugated to nanoparticles that serve as carriers for a therapeutic agent and have been used to increase the specific toxicity of tumor therapy by specific delivery to target cells, including folic acid (Pinhassi et al. 2010), Arg-Gly-Asp peptides (Su et al. 2012), vitamins (Chen et al. 2010), aptamers (Neff et al. 2011), and antibodies (Mamot et al. 2003). In particular, immunoliposomes directed against EGFR ligands can increase the targeting therapeutic efficacy in vivo and may be of important clinical significance as a novel treatment for cancer (Mamot et al. 2005). Previous studies also revealed that rapid internalization of the receptor ligand can occur upon binding to EGFR (Brand et al. 2011) and that PEGylation at the surface of nanoparticles can increase the half-life of the nanoparticles in vivo (Gupta and Torchilin 2007).

The currently available targeting radiotherapies (e.g., radionuclide-labeled monoclonal antibodies and peptides) have some limitations in targeted radionuclide therapy, such as the insufficient delivery of radionuclides to the tumor tissue because of the relatively low and heterogeneous expression of receptors on tumor cells and the dose-limiting toxicities to normal tissues. Innovative radionuclide nanoparticle delivery systems can improve and enhance the targeted transport of cytotoxic drugs or radionuclides to tumor lesions, maximize the therapeutic index, and minimize the toxicity. Five approaches are generally used for labeling or encapsulating radionuclides on nanoparticles: labeling nanocarriers by encapsulation during preparation, nanocarrier surface labeling after preparation, nanocarrier surface labeling of bioconjugates after preparation, incorporation into the lipid bilayer after preparation, and afterloading of the aqueous phase of nanocarriers after preparation (Ting et al. 2010). In the present research, we used the technique of nanocarrier surface labeling after preparation. The use of active targeting radionuclide nanoparticles in internal radiotherapy has been successfully employed to image and treat tumor models preclinically. These radionuclide nanoparticles include human atherosclerotic plaque-specific peptide-1-targeted ^{111}In-labeled liposomes (Yang et al. 2012), monoclonal antinuclear autoantibody 2C5 (mAb 2C5) targeting ^{111}In-immunoliposome for lung carcinoma (Elbayoumi et al. 2007), $\alpha_v\beta_3$-integrin-targeted ^{111}In perfluorocarbon nanoparticles for targeted tumor imaging (Hu et al. 2007), rituximab targeting ^{111}In carbon nanotubes for targeted tumor imaging (McDevitt et al. 2007), RGD- or VEGF-targeted ^{64}Cu quantum dots or iron oxide for PET/NIRF and PET/MRI imaging (Chen et al. 2008; Lee et al. 2008), EGFR-targeted ^{99m}Tc-chelated quantum dots for breast cancer imaging and therapy (Jung et al. 2011), RGD-targeted ^{125}I-labeled gold nanoparticles for tumor imaging (Kim et al. 2011), HER2-targeted nanoparticles loaded with an ^{125}I-labeled DNA intercalator (Fondell et al. 2011), anti-prostate-specific membrane antigen nanoparticles loaded with ^{225}Ac for potential targeted

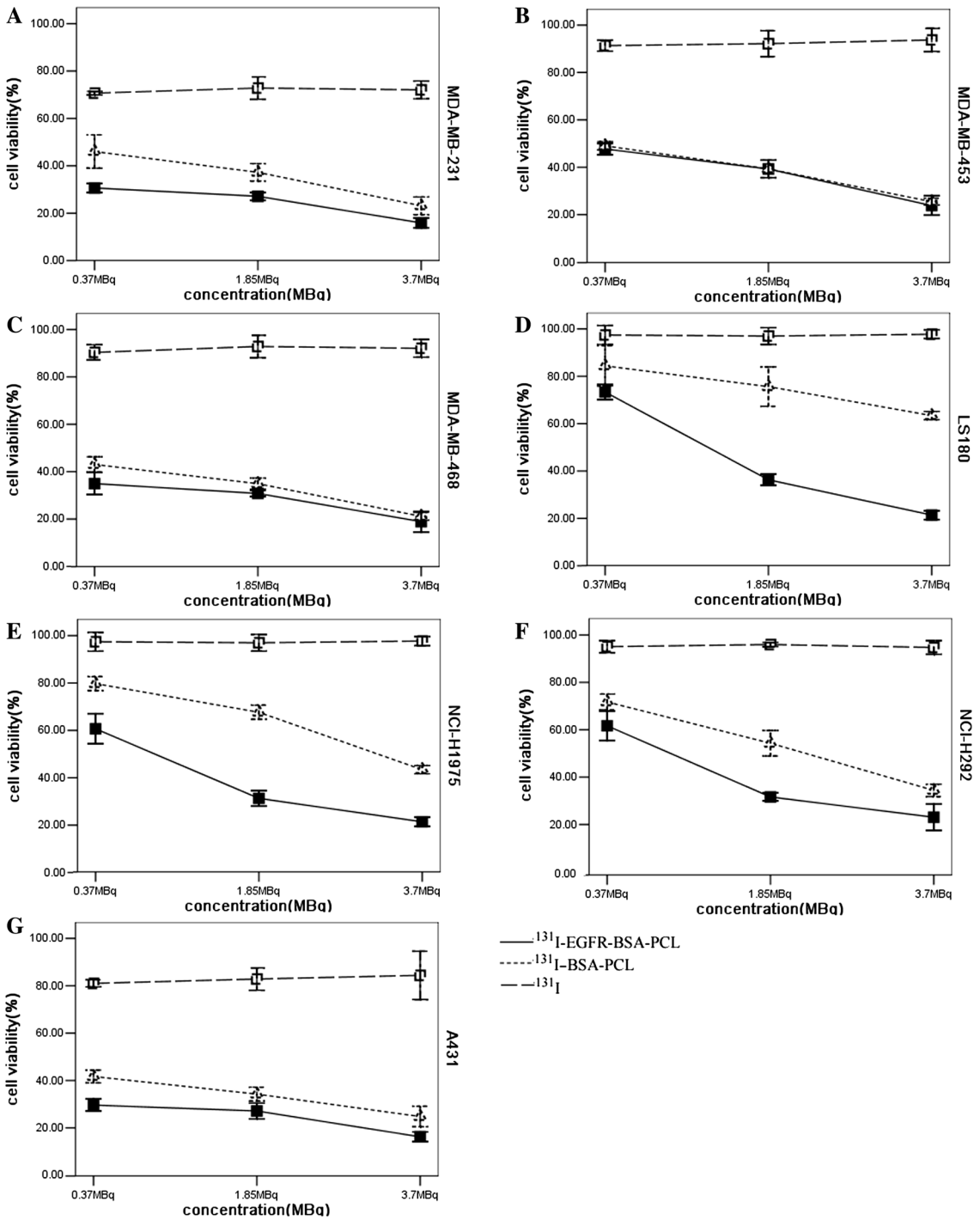

Fig. 6 In vitro cytotoxicity of ^{131}I–EGFR–BSA–PCL and ^{131}I–BSA–PCL. ^{131}I was labeled to EGFR–BSA–PCL and BSA–PCL using the chloramine-T method. Cells were treated for 12 h with ^{131}I–EGFR–BSA–PCL and ^{131}I–BSA–PCL, incubated for 1 day, and counted using the MTT assay. MDA-MB-231 (**a**), MDA-MB-453 (**b**), MDA-MB-468 (**c**), LS180 (**d**), NCI-H1975 (**e**), NCI-H292 (**f**), and A431 (**g**). ($^{*}p < 0.01$, compared with ^{131}I–BSA–PCL; $^{\#}p > 0.05$, compared with ^{131}I–BSA–PCL)

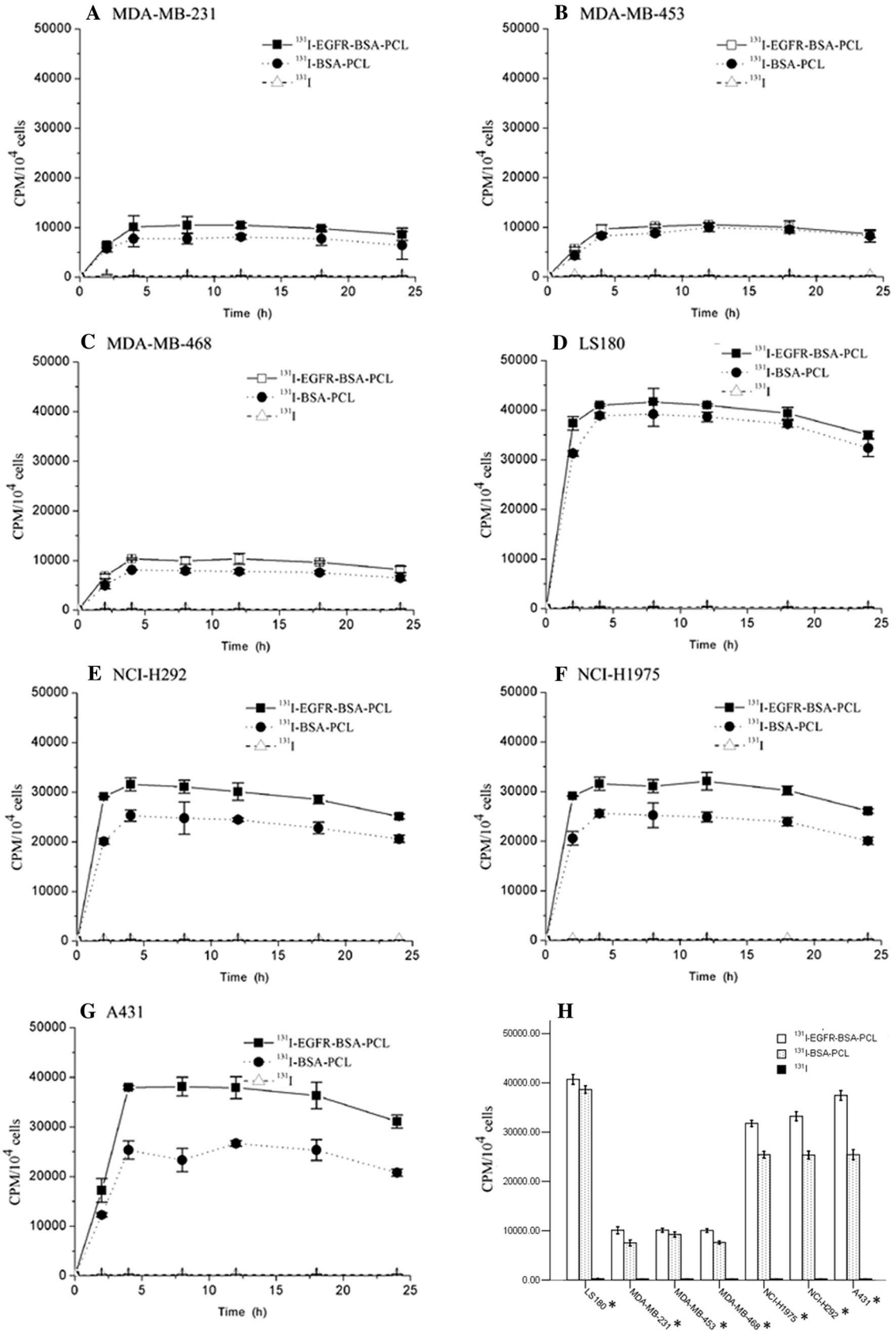
A MDA-MB-231
B MDA-MB-453
C MDA-MB-468
D LS180
E NCI-H292
F NCI-H1975
G A431
H
131I-EGFR-BSA-PCL
131I-BSA-PCL
131I
CPM/10^4 cells
Time (h)
LS180 *
MDA-MB-231 *
MDA-MB-453 *
MDA-MB-468 *
NCI-H1975 *
NCI-H292 *
A431 *

◀ **Fig. 7** Time-dependent uptake and maximal uptake of ^{131}I in different cell lines. The maximum ^{131}I uptake for these seven cell lines was obtained after 4 h of incubation with ^{131}I–EGFR–BSA–PCL and ^{131}I–BSA–PCL, but the highest cpm levels were different. The ^{131}I uptake of ^{131}I–EGFR–BSA–PCL was higher than that of ^{131}I–BSA–PCL. The remaining intracellular retention radioactivity for ^{131}I–EGFR–BSA–PCL and ^{131}I–BSA–PCL was almost 100 % after 24 h of incubation. The mean values and standard deviations are shown. MDA-MB-231 (**a**), MDA-MB-453 (**b**), MDA-MB-468 (**c**), LS180 (**d**), NCI-H1975 (**e**), NCI-H292 (**f**), and A431 (**g**). Maximal ^{131}I uptake assays in different cell lines (**h**) (*$p < 0.01$, compared with ^{131}I–BSA–PCL)

anti-vascular α-particle therapy (Bandekar et al. 2014), ^{76}Br-labeled RGD-directed-dendritic nanoprobes for PET imaging (Almutairi et al. 2009), and integrin antagonist or anti-Flk-1 antibody-coated ^{90}Y-labeled nanoparticles (Li et al. 2004).

Radionuclide nanoparticles have other advantages; they do not require a homogeneous distribution because emitting radionuclides (such as ^{131}I) can provide remote killing of cancer cells and they can tolerate imaging during treatment. For targeted radionuclide internal radiotherapy applications, high energy and low energy between 0.1 and 2.2 MeV of β-emitters are ideal radioisotopes for the treatment of small-to-large clusters of tumor cells; the maximum tissue penetration range (1–10 mm) and cross-fire effects of β-particles can kill tumor cells in close proximity to the neovasculature (Carlsson et al. 2003; Milenic et al. 2004; Mitra et al. 2006). Several β-emitting radioisotopes, such as ^{131}I, ^{90}Y, ^{186}Re, and ^{177}Lu, have been used to treat cancer for many years (Ting et al. 2010). Iodine-131 is an ideal radionuclide for therapeutic use because of its maximum β emission of 0.64 MeV with a long physical half-life of 8 days and a γ emission of 364 keV for imaging purposes in the current study. Moreover, ^{131}I radioiodine therapy for differentiated thyroid carcinomas has been used for numerous years. Given the bystander effect of radiation therapy, radioiodine may kill not only the tumor cells with uptake of radionuclide nanoparticles but also adjacent tumor cells. Although ^{131}I-labeled anti-EGFR antibody-targeted radiotherapy has been reported, EGFR-targeted ^{131}I-labeled nanoparticle radiotherapy in tumor cell lines has not yet been reported.

In the present paper, we describe for the first time a detailed study showing that EGFR-targeted ^{131}I-labeled nanoparticles allowed the evaluation of tumor targeting and therapeutic efficacy in vitro. Nanoparticles were constructed with anti-EGFR mAb fragments (C225) to deliver drugs selectively to tumor cells with EGFR overexpression. Using flow cytometry and confocal microscopy analysis, the EGFR-targeted nanoparticle EGFR–BSA–PCL showed specific binding and internalization in the EGFR-overexpressing cell lines MDA-MB-468, MDA-MB-453, and MDA-MB-468 (breast cancer); NCI-H292 and NCI-H1975 (lung cancer); LS180 (colorectal cancer); and A431 (squamous cell carcinoma). Using confocal microscopy, the selectivity for tumor cells was confirmed by revealing strong and specific binding of EGFR–BSA–PCL to targeted cancer cells. Flow cytometry revealed results consistent with those observed in fluorescent microscopy analyses, showing a significant uptake of EGFR–BSA–PCL. Moreover, the total cellular uptake of EGFR–BSA–PCL in these cells was higher than that of non-targeted nanoparticles in MDA-MB-231, MDA-MB-453, MDA-MB-468, NCI-H292, NCI-H1975, LS180, and A431 cell lines ($p < 0.05$). This finding indicates that the targeting ability of EGFR–BSA–PCL to tumor cells was enhanced via EGFR modification, resulting in EGFR receptor-mediated endocytosis.

In MTT assays, ^{131}I–EGFR–BSA–PCL was found to selectively kill EGFR-overexpressed tumor cells in a dose-dependent manner after incubation with radionuclide nanoparticles for 4 h. All of the nanoparticles were wiped off and the cells were incubated for another 24 h. The value of ^{131}I–EGFR–BSA–PCL IC50 in EGFR-overexpressed tumor cells was lower than that of ^{131}I–BSA–PCL. The cytotoxicity of ^{131}I–EGFR–BSA–PCL was found to be dependent on the radiation dose and was higher than that with the non-targeted nanoparticle ^{131}I–BSA–PCL. The survival rates of ^{131}I–EGFR–BSA–PCL were lower than those of ^{131}I–BSA–PCL in all tumor cells. Notably, no toxicity was observed when EGFR low expressing cells were incubated with the same nanoparticle. The toxic effects of EGFR–BSA–PCL and BSA–PCL were very low, as previously described against the glioma cell line U87 (Liu et al. 2014).

In the time-dependent cellular uptake experiments of ^{131}I-labeled nanoparticle nanoparticles, the data showed that ^{131}I–EGFR–BSA–PCL exhibited increased ^{131}I accumulation, and the intracellular ^{131}I retention of ^{131}I–EGFR–BSA–PCL was higher than that of ^{131}I–BSA–PCL because the EGFR-targeted nanoparticles demonstrated superior cellular binding and enhanced cellular uptake. The cells incubated with ^{131}I–BSA–PCL also showed intracellular retention of iodine, but the retention was lower in ^{131}I–BSA–PCL than that in ^{131}I–EGFR–BSA–PCL. PEGylation at the surface of nanoparticles has been well documented to increase the half-life of the nanoparticles (Gupta and Torchilin 2007). Thus, the cell-associated ^{131}I activity after 24 h was still very high, at almost 79–84 % in all seven cell lines. The ^{131}I-labeled nanoparticles showed excellent slow-release effects and better-targeted cell killing with ^{131}I. These nanoparticles may be used in preparations for future nude mice studies in vivo.

The high loco-regional retention rate led to good therapeutic results in the radioiodine therapy study in mice. In this study, we were able to deliver 74 MBq of radiation for the ^{131}I–EGFR–BSA–PCL and ^{131}I–BSA–PCL

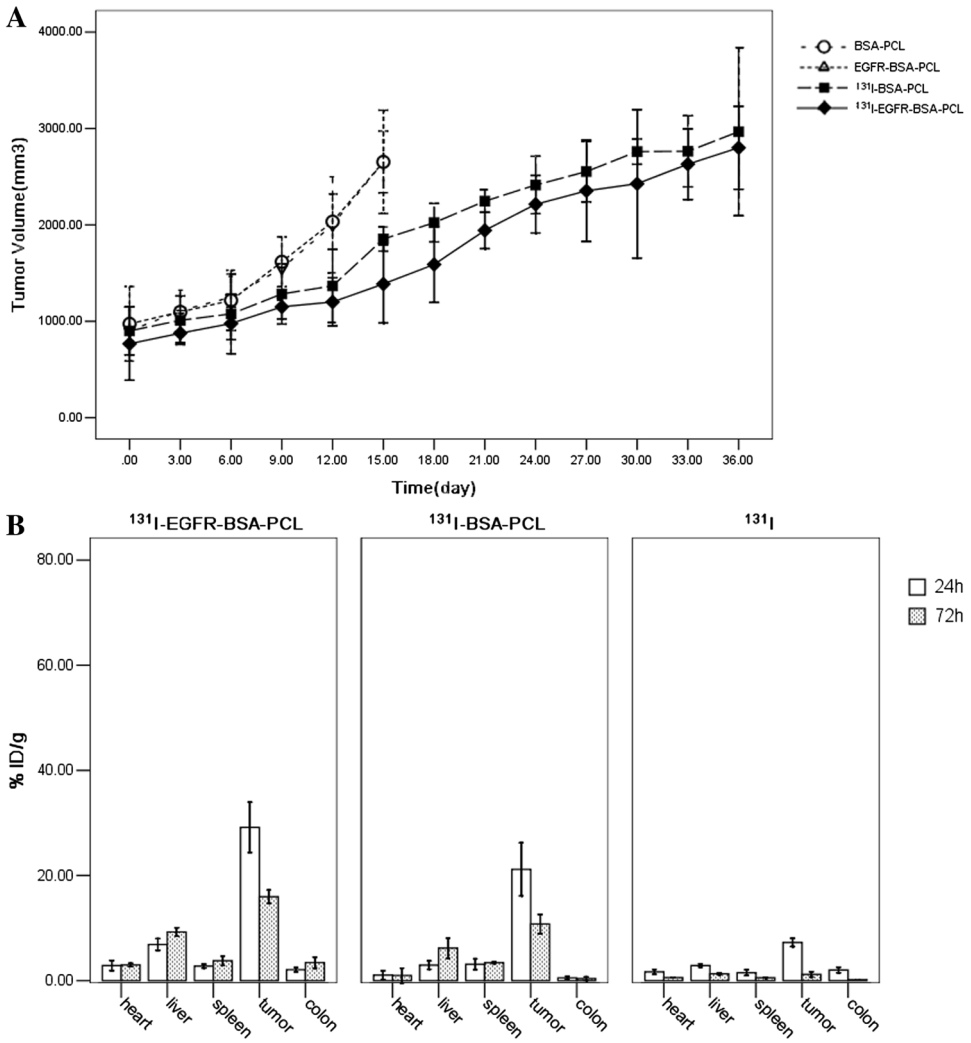

Fig. 8 Changes in the tumor volume in NCI-H1972 xenograft nude mice and tissue distribution. **a** The changes in the tumor volume in NCI-H1972 xenograft nude mice. The average tumor volumes at 35 days from the day of nanoparticle injection for the BSA–PCL, EGFR–BSA–PCL, ^{131}I–BSA–PCL, and ^{131}I–EGFR–BSA–PCL therapy groups. The two control groups showed progressive tumor growth; in contrast, the therapy groups showed slow tumor growth ($n = 5$). In comparison, tumors in the EGFR–BSA–PCL and BSA–PCL nanoparticle control groups showed rapid growth, and the tumor volumes were similar at day 15 ($p > 0.5$). On day 15, the average tumor volumes of the ^{131}I–EGFR–BSA–PCL groups were lower than ^{131}I–BSA–PCL, showing slow growth ($^{*}p < 0.01$). However, on day 35, the average tumor volumes of the ^{131}I–EGFR–BSA–PCL and ^{131}I–BSA–PCL groups were also similar ($^{\#}p = 0.5$). **b** Tissue distribution of ^{131}I–EGFR–BSA–PCL, ^{131}I–BSA–PCL, and ^{131}I. ^{131}I–EGFR–BSA–PCL and ^{131}I–BSA–PCL were markedly absorbed by tumor tissues. The tissue distribution assay revealed that ^{131}I–EGFR–BSA–PCL and ^{131}I–BSA–PCL reached their maximal uptake rate (15.96 ± 1.01 %ID/g^{-1}) and (10.79 ± 1.46 %ID/g^{-1}) at 24 h after therapy, respectively

nanoparticle groups. The two control groups showed no response regarding the unlabeled nanoparticles and showed relentless tumor enlargement. The average tumor volumes of the ^{131}I–EGFR–BSA–PCL group was lower than those of the ^{131}I–BSA–PCL groups in a mid-stage experiment because EGFR-targeted nanoparticles increased tumor cell binding and uptake and led to stronger cell killing with ^{131}I. However, the effect of radioiodine therapy became weaker with extended time, so the average tumor volumes of the ^{131}I–EGFR–BSA–PCL group were similar at the end of the experiment. The data showed that ^{131}I therapy could retard tumor growth in a mid-stage experiment. The difference between the tumor size of the ^{131}I–EGFR–BSA–PCL and ^{131}I–BSA–PCL nanoparticle groups was most likely due to EGFR-targeted liposomes increasing tumor cellular binding and uptake. Although intravenous injection of nanoparticles would be simpler and better than intratumoral injection in the radioiodine therapy study in mice, the data for intravenous injection showed that the nanoparticles were mostly retained in the liver and

spleen, secondary to the tumor; thus, the treatment effect of ^{131}I-labeled nanoparticles was poor in vivo. In the in vivo radioiodine therapy study, EGFR-targeted ^{131}I-labeled nanoparticles had a favorable biological half-life and retarded tumor growth to some extent, but the effect of radioiodine therapy was decreased with time. This may be because ^{131}I did not have enough radiation energy; thus, more powerful radionuclides instead of ^{131}I in EGFR-targeted nuclide nanoparticles could be used in future research.

In conclusion, EGFR–BSA–PCL exhibited superior cellular binding and enhanced cellular uptake compared with the control BSA–PCL. Furthermore, ^{131}I–EGFR–BSA–PCL achieved a favorable intracellular retention of ^{131}I, excellent targeted cell killing, and slow-release effects, and it suppressed the cancer cell growth caused by EGFR overexpression. The radionuclide-targeted anti-EGFR nanoparticle ^{131}I–EGFR–BSA–PCL is a good candidate for targeted drug delivery purposes in EGFR-targeted therapeutic approaches for ^{131}I radioiodine treatment for breast cancer, lung cancer, colorectal cancer, and squamous cell carcinoma cell lines.

Acknowledgments This study was supported by Grants from the National Natural Science Foundation of China (to Jian TAN) (No. 81171372) (to Wei LI) (No. 81301244), Tianjin Research Program of Application Foundation and Advanced Technology (to Tong LIU) (No. 11JCYBJC11700) and the National Key Clinical Specialty Project of China.

Compliance with ethical standards

Conflict of interest This paper is our own work; we have no specific disclaimers or conflicts of interest.

Ethical approval This study was carried out in strict accordance with the recommendations in the Guide for the Care and Use of Laboratory Animals of the National Institutes of Health and China Regulations For the Administration of Affairs Concerning Experimental Animals. The protocol was approved by the Committee on the Ethics of Animal Experiments of the Tianjin Medical University General Hospital. All surgery was performed under sodium pentobarbital anesthesia, and all efforts were made to minimize suffering.

References

Almutairi A, Rossin R, Shokeen M, Hagooly A, Ananth A, Capoccia B, Guillaudeu S, Abendschein D, Anderson CJ, Welch MJ, Frechet JM (2009) Biodegradable dendritic positron-emitting nanoprobes for the noninvasive imaging of angiogenesis. Proc Natl Acad Sci USA 106:685–690

Ang KK, Berkey BA, Tu X, Zhang HZ, Katz R, Hammond EH, Fu KK, Milas L (2002) Impact of epidermal growth factor receptor expression on survival and pattern of relapse in patients with advanced head and neck carcinoma. Cancer Res 62:7350–7356

Bandekar A, Zhu C, Jindal R, Bruchertseifer F, Morgenstern A, Sofou S (2014) Anti-prostate-specific membrane antigen liposomes loaded with 225Ac for potential targeted antivascular alpha-particle therapy of cancer. J Nucl Med 55:107–114

Brand TM, Iida M, Li C, Wheeler DL (2011) The nuclear epidermal growth factor receptor signaling network and its role in cancer. Discov Med 12:419–432

Capelan M, Pugliano L, De Azambuja E, Bozovic I, Saini KS, Sotiriou C, Loi S, Piccart-Gebhart MJ (2013) Pertuzumab: new hope for patients with HER2-positive breast cancer. Ann Oncol 24:273–282

Carlsson J, Forssell Aronsson E, Hietala SO, Stigbrand T, Tennvall J (2003) Tumour therapy with radionuclides: assessment of progress and problems. Radiother Oncol 66:107–117

Chen K, Li ZB, Wang H, Cai W, Chen X (2008) Dual-modality optical and positron emission tomography imaging of vascular endothelial growth factor receptor on tumor vasculature using quantum dots. Eur J Nucl Med Mol Imaging 35:2235–2244

Chen S, Zhao X, Chen J, Kuznetsova L, Wong SS, Ojima I (2010) Mechanism-based tumor-targeting drug delivery system. Validation of efficient vitamin receptor-mediated endocytosis and drug release. Bioconjug Chem 21:979–987

Chen CL, Hu GY, Mei Q, Qiu H, Long GX, Hu GQ (2012) Epidermal growth factor receptor-targeted ultra-small superparamagnetic iron oxide particles for magnetic resonance molecular imaging of lung cancer cells in vitro. Chin Med J (Engl) 125:2322–2328

Chen Y, Peng J, Han M, Omar M, Hu D, Ke X, Lu N (2015) A low-molecular-weight heparin-coated doxorubicin-liposome for the prevention of melanoma metastasis. J Drug Target 23:335–346

Cho YS, Yoon TJ, Jang ES, Soo Hong K, Young Lee S, Ran Kim O, Park C, Kim YJ, Yi GC, Chang K (2010) Cetuximab-conjugated magneto-fluorescent silica nanoparticles for in vivo colon cancer targeting and imaging. Cancer Lett 299:63–71

Chung TH, Hsiao JK, Hsu SC, Yao M, Chen YC, Wang SW, Kuo MY, Yang CS, Huang DM (2011) Iron oxide nanoparticle-induced epidermal growth factor receptor expression in human stem cells for tumor therapy. ACS Nano 5:9807–9816

Du C, Deng D, Shan L, Wan S, Cao J, Tian J, Achilefu S, Gu Y (2013) A pH-sensitive doxorubicin prodrug based on folate-conjugated BSA for tumor-targeted drug delivery. Biomaterials 34:3087–3097

Elbayoumi TA, Pabba S, Roby A, Torchilin VP (2007) Antinucleosome antibody-modified liposomes and lipid-core micelles for tumor-targeted delivery of therapeutic and diagnostic agents. J Liposome Res 17:1–14

Fondell A, Edwards K, Unga J, Kullberg E, Park JW, Gedda L (2011) In vitro evaluation and biodistribution of HER2-targeted liposomes loaded with an (125)I-labelled DNA-intercalator. J Drug Target 19:846–855

Giaccone G (2005) HER1/EGFR-targeted agents: predicting the future for patients with unpredictable outcomes to therapy. Ann Oncol 16:538–548

Gupta B, Torchilin VP (2007) Monoclonal antibody 2C5-modified doxorubicin-loaded liposomes with significantly enhanced therapeutic activity against intracranial human brain U-87 MG tumor xenografts in nude mice. Cancer Immunol Immunother 56:1215–1223

Hu G, Lijowski M, Zhang H, Partlow KC, Caruthers SD, Kiefer G, Gulyas G, Athey P, Scott MJ, Wickline SA, Lanza GM (2007) Imaging of Vx-2 rabbit tumors with alpha(nu)beta3-integrin-targeted ^{111}In nanoparticles. Int J Cancer 120:1951–1957

Hussain AF, Kruger HR, Kampmeier F, Weissbach T, Licha K, Kratz F, Haag R, Calderon M, Barth S (2013) Targeted delivery of dendritic polyglycerol–doxorubicin conjugates by scFv-SNAP fusion protein suppresses EGFR+ cancer cell growth. Biomacromolecules 14:2510–2520

Jung KH, Choe YS, Paik JY, Lee KH (2011) 99mTc-Hydrazinonicotinamide epidermal growth factor-polyethylene glycol-quantum dot imaging allows quantification of breast cancer epidermal growth factor receptor expression and monitors receptor

downregulation in response to cetuximab therapy. J Nucl Med 52:1457–1464

Kao HW, Lin YY, Chen CC, Chi KH, Tien DC, Hsia CC, Lin MH, Wang HE (2013) Evaluation of EGFR-targeted radioimmunogold-nanoparticles as a theranostic agent in a tumor animal model. Bioorg Med Chem Lett 23:3180–3185

Kim YH, Jeon J, Hong SH, Rhim WK, Lee YS, Youn H, Chung JK, Lee MC, Lee DS, Kang KW, Nam JM (2011) Tumor targeting and imaging using cyclic RGD-PEGylated gold nanoparticle probes with directly conjugated iodine-125. Small 7:2052–2060

Lee HY, Li Z, Chen K, Hsu AR, Xu C, Xie J, Sun S, Chen X (2008) PET/MRI dual-modality tumor imaging using arginine-glycine-aspartic (RGD)-conjugated radiolabeled iron oxide nanoparticles. J Nucl Med 49:1371–1379

Li L, Wartchow CA, Danthi SN, Shen Z, Dechene N, Pease J, Choi HS, Doede T, Chu P, Ning S, Lee DY, Bednarski MD, Knox SJ (2004) A novel antiangiogenesis therapy using an integrin antagonist or anti-Flk-1 antibody coated 90Y-labeled nanoparticles. Int J Radiat Oncol Biol Phys 58:1215–1227

Liu Z, Dong C, Wang X, Wang H, Li W, Tan J, Chang J (2014) Self-assembled biodegradable protein-polymer vesicle as a tumor-targeted nanocarrier. ACS Appl Mater Interfaces 6:2393–2400

Mamot C, Drummond DC, Greiser U, Hong K, Kirpotin DB, Marks JD, Park JW (2003) Epidermal growth factor receptor (EGFR)-targeted immunoliposomes mediate specific and efficient drug delivery to EGFR- and EGFRvIII-overexpressing tumor cells. Cancer Res 63:3154–3161

Mamot C, Drummond DC, Noble CO, Kallab V, Guo Z, Hong K, Kirpotin DB, Park JW (2005) Epidermal growth factor receptor-targeted immunoliposomes significantly enhance the efficacy of multiple anticancer drugs in vivo. Cancer Res 65:11631–11638

Mamot C, Ritschard R, Kung W, Park JW, Herrmann R, Rochlitz CF (2006) EGFR-targeted immunoliposomes derived from the monoclonal antibody EMD72000 mediate specific and efficient drug delivery to a variety of colorectal cancer cells. J Drug Target 14:215–223

McDevitt MR, Chattopadhyay D, Kappel BJ, Jaggi JS, Schiffman SR, Antczak C, Njardarson JT, Brentjens R, Scheinberg DA (2007) Tumor targeting with antibody-functionalized, radiolabeled carbon nanotubes. J Nucl Med 48:1180–1189

Milenic DE, Brady ED, Brechbiel MW (2004) Antibody-targeted radiation cancer therapy. Nat Rev Drug Discov 3:488–499

Mitra A, Nan A, Line BR, Ghandehari H (2006) Nanocarriers for nuclear imaging and radiotherapy of cancer. Curr Pharm Des 12:4729–4749

Nagaria TS, Williams JL, Leduc C, Squire JA, Greer PA, Sangrar W (2013) Flavopiridol synergizes with sorafenib to induce cytotoxicity and potentiate antitumorigenic activity in EGFR/HER-2 and mutant RAS/RAF breast cancer model systems. Neoplasia 15:939–951

Neff CP, Zhou J, Remling L, Kuruvilla J, Zhang J, Li H, Smith DD, Swiderski P, Rossi JJ, Akkina R (2011) An aptamer-siRNA chimera suppresses HIV-1 viral loads and protects from helper CD4(+) T cell decline in humanized mice. Sci Transl Med 3:66ra66

Nordberg E, Friedman M, Gostring L, Adams GP, Brismar H, Nilsson FY, Stahl S, Glimelius B, Carlsson J (2007) Cellular studies of binding, internalization and retention of a radiolabeled EGFR-binding affibody molecule. Nucl Med Biol 34:609–618

Normanno N, Tejpar S, Morgillo F, De Luca A, Van Cutsem E, Ciardiello F (2009) Implications for KRAS status and EGFR-targeted therapies in metastatic CRC. Nat Rev Clin Oncol 6:519–527

Pastorino F, Brignole C, Marimpietri D, Sapra P, Moase EH, Allen TM, Ponzoni M (2003) Doxorubicin-loaded Fab' fragments of anti-disialoganglioside immunoliposomes selectively inhibit the growth and dissemination of human neuroblastoma in nude mice. Cancer Res 63:86–92

Pinhassi RI, Assaraf YG, Farber S, Stark M, Ickowicz D, Drori S, Domb AJ, Livney YD (2010) Arabinogalactan-folic acid-drug conjugate for targeted delivery and target-activated release of anticancer drugs to folate receptor-overexpressing cells. Biomacromolecules 11:294–303

Saha RN, Vasanthakumar S, Bende G, Snehalatha M (2010) Nanoparticulate drug delivery systems for cancer chemotherapy. Mol Membr Biol 27:215–231

Su W, Wang H, Wang S, Liao Z, Kang S, Peng Y, Han L, Chang J (2012) PEG/RGD-modified magnetic polymeric liposomes for controlled drug release and tumor cell targeting. Int J Pharm 426:170–181

Ting G, Chang CH, Wang HE, Lee TW (2010) Nanotargeted radionuclides for cancer nuclear imaging and internal radiotherapy. J Biomed Biotechnol 2010:1–17. doi:10.1155/2010/953537

Yang FY, Wang HE, Liu RS, Teng MC, Li JJ, Lu M, Wei MC, Wong TT (2012) Pharmacokinetic analysis of 111 in-labeled liposomal Doxorubicin in murine glioblastoma after blood-brain barrier disruption by focused ultrasound. PLoS ONE 7:e45468

Zhou X, Qiu J, Wang Z, Huang N, Li X, Li Q, Zhang Y, Zhao C, Luo C, Zhang N, Teng X, Chen Z, Liu X, Yu X, Wu W, Wei YQ, Li J (2012) In vitro and in vivo anti-tumor activities of anti-EGFR single-chain variable fragment fused with recombinant gelonin toxin. J Cancer Res Clin Oncol 138:1081–1090